Atomic scale study of InP etching by Cl-Ar ICP plasma discharge

A. Rhallabi, R. Chanson, J.-P. Landesman, Christophe Cardinaud, M.-C. Fernandez

Atomic scale study of InP etching by Cl_2-Ar ICP plasma discharge

Ahmed Rhallabi, Romain Chanson, Jean Pierre Landesman, Christophe Cardinaud, Marie-Claude Fernandez

Institut des Matériaux Jean Rouxel, CNRS - Université de Nantes, France

Abstract

A gas phase kinetic model combined to a 3D atomic etching model have been developed to study the etching process of InP under Cl_2-Ar ICP plasma discharge. A gas phase global kinetic model is used to calculate the reactive particle fluxes implied in the etching mechanisms. The 3D atomic InP etching model is based on the Monte-Carlo kinetic approach where the plasma surface interactions are described in the probability way. The coupling between the plasma chemistry model and the surface etching model is an interesting approach to predict the etched surface properties in term of the etch rate, the surface roughness and surface steochiometry as a function of the operating conditions.

A satisfactory agreement is obtained by comparing the experimental and the simulation results concerning the evolution of the main plasma discharge parameters such as the electron density and temperature versus the ICP source power for surface recombination coefficient of atomic chlorine fixed at γ_{Cl}=0.04. On the other hand, simulation results show the effect of the operating conditions on the etched surface roughness and the etch rate evolutions with time in the early stage. Moreover, the simulation results show the correlation between the decrease of the ion to chlorine flux ratio and the decrease of the RRMS as a function of the pressure.

I. Introduction

Nowadays, plasma process represents one of the keys for the integration enhancement of electronic and optical devices. Indeed, it is now possible with plasma etching process using high density plasma reactors such as Inductive Coupled Plasma (ICP) to transfer nanometer scale patterns from the mask to the substrate [1-5]. The success of the high aspect ratio pattern transfer without geometrical defects [6-9] (bowing, undercut, trenching,..) is tributary of a good understanding of the physical and chemical mechanisms of the plasma discharge and the surface kinetic processes. Some attempts of Si and III-V pattern transfer development like photonic crystals, deep trenches or mesa structures are achieved by plasma etching [10-16]. For this type of devices, dry etching based on the plasma discharge is developed by using a variety of gas like Cl_2 [13-15], $SiCl_4$ [10,16], etc. Experimental studies concerning the chloride plasma discharges have been carried out to investigate the electrical and kinetic properties of mentioned plasma discharges [17-23]. Modelling of plasma discharge in different degrees of complexity, specially, for the chloride precursors have been developed by using different approaches [9,24-28] such as fluid model, Particle In Cell or global model to model the electro-magnetic phenomena transport of charged species in different types of reactors.

Some atomic approaches of surface kinetic model have been developed to study the plasma surface interaction phenomena for etching processes. The first one concerns the molecular dynamics which is based on the solving of the equation of motion for a system of interacting particles. Newton's equations of motion are integrated numerically to compute the atom's trajectory [34,35]. Such method is developed to compare physical sputtering and chemical

sputtering for the silicon etching by fluoride precursors [34]. The accurate information obtained with this method is conditioned by the good knowledge of the interaction potential functions. This method is applied for small etched surfaces because of the time consuming. The second method is based on the Monte-Carlo kinetic method [36] where the initial etched material is represented in 3D layer. Such method allowed to easily take into account of several adsorbed precursors impinging on the substrate surface and site identities during the etching process. The Monte-Carlo method was already applied to the InP etching by CH_4-H_2 plasma [36]. It allowed to show the role of both the chemisorption probabilities of CH_3 and H and the surface migration process on the phosphorus depletion in the shallow layers [36].

In this study, we have developed a kinetic model based on the global approach in which the densities of neutral and charged species produced in plasma are assumed spatially uniform [26-28]. Its advantage is to give approximate information about the reactive species transport with a reasonable simulation time. This model is applied to the Inductive Coupled Plasma (ICP) discharge of Cl_2/Ar. The model consists in the calculation of the densities of species from a set of mass balance equations describing the major gas-phase processes. The gas phase kinetic model is connected to 3D etching model in order to predict the etched InP material properties as a function of the operating conditions. 3D Monte-Carlo method is applied to follow the properties of the etched InP surface evolution with time.

In section 2, the gas phase model is described and a discussion of the kinetic reactions is presented. Results from this model are given and comparisons between the simulations and the experiments have been presented. The 3D Monte-Carlo etching model is described in section 3 and includes hypothesis justifications. The simulation results from the etching model are presented showing the interest to couple the plasma kinetic model to the etching model in the prediction of the etched surface properties versus the operating conditions. Concluding remarks are in section 4.

2. Global kinetic Model

The gas phase model is based on the time dependent resolution of the mass balance equations of main chemical species existing in the reactor. Thus, the rate equation for the primary molecules (Cl_2 and Ar in our case) with density N_i (i=Cl_2 or Ar) is given as [26-27]:

$$\frac{dNi}{dt} = x\frac{Q}{V} - \sum_l k_{el}(Te)N_i n_e + \sum_n k_{en}(Te)N_n n_e - \sum_m k_{mi}(T)N_i Nm + \sum_{lm} k_{ml}(T)N_l N_m + \sum_l ks_l N_l - \frac{Ni}{\tau_R} \qquad (1)$$

where the first term represents the source term which Q is the total flow rate, V is the reactor volume, x is the fraction of the primary molecule (Cl_2 or Ar) and τ_R is the residence time of molecules in reactor. The second term represents the loss rate of chlorine/argon by electron impact which k_{el} is the kinetic constant of the l^{th} reaction by electron impact with the molecule (i). The third term is the production rate of chlorine/argon by electron impact with species (n). The fourth term is the loss rate of chlorine/argon by reaction between (i) and (m) species. The fifth term is the production rate of the species (i) by reaction between (l) and (m) species, which k_{ml} is the kinetic constant of the reaction between (l) and (m). The sixth term is the production rate of chlorine/Argon on the surface due to the transformation of the species (l) to (i). For Ar, $\sum_l k_{sl} N_l = k_{21}\left[A_r^*\right] + k_{20}\left[A_r^+\right]$ while for Cl_2, $\sum_l k_{sl} N_l = \frac{1}{2}k_{17}[Cl] + k_{19}\left[Cl_2^+\right]$ (see table 1). The last term is the loss rate by pumping. T and T_e are the gas and electron temperatures respectively. For the other neutral and ion species the balance equations are given as [26-27]:

$$\frac{dN_j}{dt} = -\sum_l k_l(Te)N_j n_e + \sum_n k_n(Te)N_n n_e - \sum_m k_{mj}(T)N_j Nm + \sum_{lm} k_{ml}(T)N_l N_m - ks_j N_j + \sum_l ks_l N_l - \frac{N_j}{\tau_R} \quad (2)$$

$ks_j N_j$ is the surface lost rate of j[th] species. For the neutral species, ks_j is determined as a function of the diffusion coefficient D_j and diffusion length Λ of the j[th] species [27]:

$$ks_j = \gamma_j \frac{D_j}{\Lambda^2} \quad (3)$$

γ_j is the recombination coefficient on the surface of the j[th] species. Λ depends on the reactor geometry parameters. For a cylindrical reactor Λ is given as [29]:

$$\frac{1}{\Lambda^2} = \left(\frac{\pi}{L}\right)^2 + \left(\frac{2.405}{R}\right)^2 \quad (4)$$

where L and R are the height and the radius of ICP reactor.
For the positive ion species, k_{sj} is given as [27]:

$$k_{sj} = 2\, u_{B,j}\left(R^2\, h_L + R\, L\, h_R\right) / R^2\, L \quad (5)$$

where $u_{B,j}$ is the Bohm velocity. h_L and h_R are the ratio of the wall density to the bulk average density of species j for the walls located in the axial and the radial directions respectively [27].

The power balance equation is added to the plasma kinetic equation system to self-consistently evaluate the electron temperature. It is given as [27,28]:

$$\frac{\partial}{\partial t}\left(\frac{3}{2} q T_e n_e\right) = P_{RF} - P_{abs} \quad (6)$$

where P_{RF} and P_{abs} are the RF power injected in the reactor and the power absorbed by plasma respectively. P_{abs} is given as [27,28]:

$$P_{abs} = P_{ev} + P_{ew} + P_{iw} \quad (7)$$

where P_{ev} is power losses for inelastic and elastic collisions by electron impact and P_{ew} and P_{iw} are power losses on the surface for electron and positive ions respectively. The addition of power equation to the kinetic system allows to self-consistently calculate the electron temperature and thus to deduce the chemical species densities as a function of the injected power in the ICP reactor.

The balance equation system is completed by the charge neutrality equation:

$$n_e + \sum_j n_j^- = \sum_j n_j^+ \quad (8)$$

where n_j^- and n_j^+ are the negative and positive ions respectively.

Table 1 shows kinetic reactions taken into account in the mass balance equations. The mass balance equations are applied to Cl_2, Cl, Cl_2^+, Cl^+, Cl^-, Ar, Ar^* and Ar^+ which are considered as the dominant species in the Cl_2/Ar plasma. Metastable states of Cl_2 and Cl are not taken into account in the kinetic system. However, the reactions involving the metastable species are considered in the power balance equation because of the significant fraction of the injected power which is lost by the excitation processes (table2).

The differential equation system composed of equations 1,2,7,8 is resolved from initial conditions until the study state when Te and all species densities become constant with time.
Tables 1-2 give the reactions taken into account in the system for the Cl_2/Ar plasma mixture. The rate constants for electron impact are calculated knowing the electron cross sections and assuming a Maxwellian distribution of electron energy [27,28,30,31,43-53].

Electron impact reactions and volume reactions		**Reaction constants, Te (eV)**	**References**
k_1	$e + Cl_2 \rightarrow Cl_2^+ + 2e$	$k_1 = 9.21\ 10^{-8}\ \exp(-12.9/Te)\ \ cm^3/s$	27, 28,30
k_2	$e + Cl_2 \rightarrow Cl^+ + Cl + 2e$	$k_2 = 3.88\ 10^{-9}\ \exp(-15.5/Te)\ \ cm^3/s$	27, 28,30
k_3	$e + Cl_2 \rightarrow Cl^+ + Cl^- + e$	$k3 = 8.55\ 10^{-10} \exp(-12.65/Te)\ cm^3/s$	27, 28,30
k_4	$e + Cl_2 \rightarrow 2Cl + e$	$k_4 = 3.80\ 10^{-8} \exp(-3.824/Te)\ \ cm^3/s$	27, 43
k_5	$e + Cl_2 \rightarrow Cl + Cl^-$	$k_5 = 3.69 10^{-10} \exp(-1.68/Te + 1.457/Te^2 - 0.44/Te^3 + 0.0572/Te^4 - 0.0026/Te^5)\ \ cm^3/s$	27, 28,30
k_6	$e + Cl \rightarrow Cl^+ + 2e$	$k_6 = (Te/12.96)^{0.5}\ \exp(-12.96/Te)\ (1.419\ 10^{-7} - 1.864\ 10^{-8} \log(Te/12.96) - 5.439 10^{-8}\ \log(Te/12.96)^2 + 3.306\ 10^{-8} \log(Te/12.96)^3 - 3.54\ 10^{-9}\ \log(Te/12.96)^4 - 2.915\ 10^{-8}\ \log(Te/12.96)^5))\ \ cm^3/s$	27,31
k_7	$Cl^- + Cl_2^+ \rightarrow Cl + Cl_2$	$k_7 = 5\times10^{-8}\ \ cm^3/s$	27,44
k_8	$Cl^- + Cl^+ \rightarrow Cl + Cl$	$k_8 = 5\times10^{-8}\ \ cm^3/s$	27,44
k_9	$e + Cl^- \rightarrow Cl + 2e$	$k_9 = 2.63\ 10^{-8} \exp(-5.37/Te)\ \ cm^3/s$	27
k_{10}	$e + Ar \rightarrow Ar^+ + 2e$	$k_{10} = 1.23\ 10^{-7} \exp(-18.68/Te)\ \ cm^3/s$	27,48
k_{11}	$e + Ar \rightarrow Ar^* + 2$	$k_{11} = 3.71\ 10^{-8} \exp(-15.06/Te)\ \ cm^3/s$	27,49
k_{12}	$e + Ar^* \rightarrow Ar^+ + 2e$	$k_{12} = 2.05\ 10^{-7} \exp(-4.95/Te)\ \ cm^3/s$	27,50
k_{13}	$e + Ar^* \rightarrow Ar + e$	$k_{13} = 2.0\ 10^{-9}\ \ cm^3/s$	27,45-47
k_{14}	$Ar^* + Ar^* \rightarrow Ar + Ar^+$	$k_{14} = 6.2\ 10^{-10}\ \ cm^3/s$	27,45-47
k_{15}	$Ar^+ + Cl^- \rightarrow Ar + Cl$	$k_{15} = 3\ 10^{-8}\ \ cm^3/s$	27
k_{16}	$Ar^* + Cl_2 \rightarrow Ar + 2Cl$	$k_{16} = 71\ 10^{-11}\ \ cm^3/s$	52,53
Surface reactions			
k_{17}	$Cl \rightarrow 1/2 Cl_2$	$k17 = \gamma_{Cl} \times D_{Cl} / \Lambda^2\ \ s$	27
k_{18}	$Cl^+ \rightarrow Cl$	$k_{18} = 2\ u_{B,Cl^+} \left(R^2\ h_L\ + R\,L\,h_R\right) / R^2\ L\ \ \ s^{-1}$	27
k_{19}	$Cl_2^+ \rightarrow Cl_2$	$k_{19} = 2\ u_{B,Cl_2^+} \left(R^2\ h_L\ + R\,L\,h_R\right) / R^2\ L\ \ \ s^{-1}$	27
k_{20}	$Ar^+ \rightarrow Ar$	$k_{20} = 2\ u_{B,Ar^+} \left(R^2\ h_L\ + R\,L\,h_R\right) / R^2\ L\ \ \ s^{-1}$	27
k_{21}	$Ar^* \rightarrow Ar$	$k_{21} = D_{Ar*} / \Lambda^2\ \ s^{-1}$	27

Table1. Kinetic reactions considered in the mass balance equations.

Electron impact reactions and volume reactions		Reaction constants, Te (eV)	Ref
k_{22}	$e + Cl_2 \rightarrow Cl_2(b^3\Pi_u) + e$	$k_{22} = 6.13\,10^{-10}\ \exp(2.74/Te - 6.85/Te^2 + 3.69/Te^3 - 0.856/Te^4 + 0.0711/Te^5)$	27
k_{23}	$e + Cl_2 \rightarrow Cl_2(^1\Pi_u) + e$	$k_{23} = 3.80\,10^{-8}\ \exp(-3.824/Te)$	27
k_{24}	$e + Cl_2 \rightarrow Cl_2(^1\Pi_g) + e$	$k_{24} = 9.74\,10^{-9}\ \exp(-10.71/Te)$	27
k_{25}	$e + Cl_2 \rightarrow Cl_2(^1\Sigma_u) + e$	$k_{25} = 2.12\,10^{-9}\ \exp(-11.16/Te)$	27
k_{26}	$e + Cl_2 \rightarrow Cl_2 + e$ (momentum transfert)	$k_{26} = 4.47\,10^{-7}\ \exp(-2.17/Te + 0.362/Te^2 - 0.0196/Te^3)$	27
k_{27}	$e + Cl_2 \rightarrow Cl_2 + e$ (vibrational excitation)	$k_{27} = 9.26\,10^{-10}\ \exp(5.85/Te - 4.94/Te^2 + 1.716/Te^3 - 0.251/Te^4 + 0.123/Te^5)$	27
k_{28}	$e + Cl \rightarrow Cl(^3D) + e$	$k_{28} = 1.99\,10^{-8}\ \exp(-10.06/Te)$	27,51
k_{29}	$e + Cl \rightarrow Cl(^4D) + e$	$k_{29} = 9.24\,10^{-9}\ \exp(-11.15/Te)$	27,51
k_{30}	$e + Cl \rightarrow Cl(^4P) + e$	$k_{30} = 1.60\,10^{-8}\ \exp(-10.29/Te)$	27
k_{31}	$e + Cl \rightarrow Cl(^4S) + e$	$k_{31} = 1.27\,10^{-8}\ \exp(-10.97/Te)$	27,51
k_{32}	$e + Cl \rightarrow Cl(^5D) + e$	$k_{32} = 5.22\,10^{-9}\ \exp(-11.12/Te)$	27,51
k_{33}	$e + Cl \rightarrow Cl(^5P) + e$	$k_{33} = 2.79\,10^{-9}\ \exp(-11.06/Te)$	27

Table 2. Kinetic reactions of excitation of both Cl_2 and Cl which are added in the mass balance power equation.

The results of the 0D global plasma model have been compared to electron density and temperature measurements performed in a Sentech SI 500 ICP etch system used to etch III-V materials, and customized to integrate electrical and optical diagnostics [41, 42]. The ICP source consists of a planar antenna with an Al_2O_3 coupling window. The reactor chamber is made of un-anodised aluminum. The height from coupling window to electrode surface is of ~130mm and the internal chamber diameter is of 350 mm. A c-Al_2O_3 wafer was used as the (un-biased) electrode coverplate during measurements. Details of the experimental procedure can be found in [43]. The RF-compensated Langmuir probe was positioned ~ 35 mm above the electrode surface [*and ~ 130 mm away from the reactor center]* during the measurements. The surface recombination coefficient of Cl atoms γ_{Cl} in the reactor was estimated using the PIF method [42] and was found to be lie in the range of 0.03-0.05 for ICP powers in the range of 150 W – 800 W, at 10 mT pressure. Except for the study of the effect of the γ_{Cl} on the Cl_2-Ar kinetic plasma properties (figures 6-9), the simulations are carried out for γ_{Cl} =0.04.

Figure 1 shows the electron density evolution with power for different pressure and pressure values. For different gas pressures, electron density increases with power because of the increase of the ionisation rate. At low power [ne] decreases with pressure. This characterises the electronegative plasma. However, over 400 watt, the electron density increases with the pressure. We can observe that the electronegativity of Cl_2/Ar represented by the ratio $[Cl^-]/[n_e]$ decreases with RF power (figure 2). $[Cl^-]/[n_e]$ is sensitive to the pressure for P_{rf} lower than 400 watt Beyond this value, $[Cl^-]/[n_e]$ becomes less sensitive to the pressure variations.

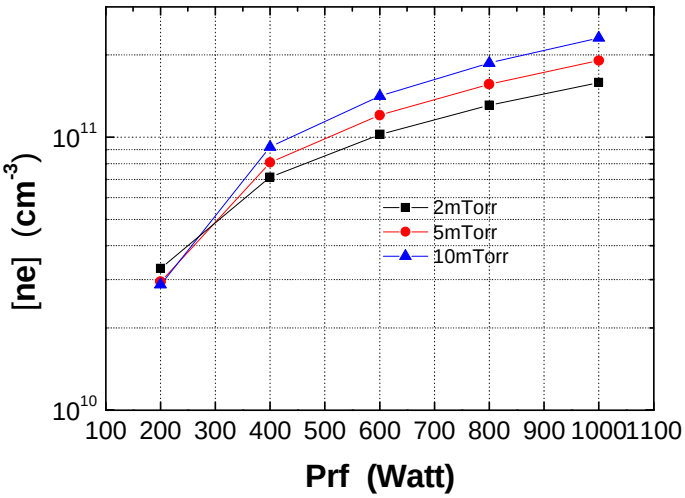

Figure 1. Variation of electron density with power for pressure ranging from 2 to 10 mtorr, Q(Cl_2/Ar

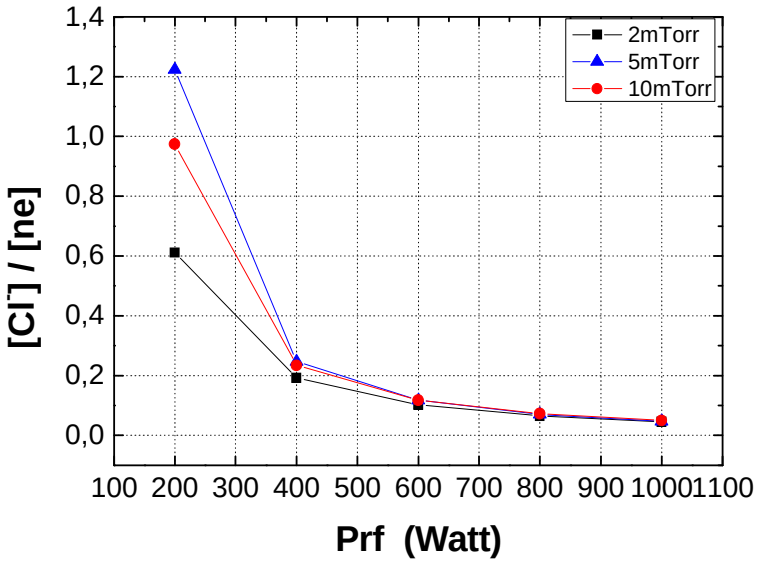

Figure 2. Variation of Cl^- ion to electron density ratio with power for pressure ranging from 2 to 10 mtorr, Q(Cl_2/Ar)=10:10 sccm.

The variation of the electron temperature for different values of pressure is presented in figure 3. For the pressure ranging from 2 to 10 mtorr, T_e decreases as a function of power for Prf <400 Watt. In this power interval, the augmentation of power has more effect in the production of electrons by ionization processes (figure 1) leading to the diminution of electron energy. However, for a high power values one fraction of power causes the acceleration of electrons leading to the increase of their average energy (electron temperature).

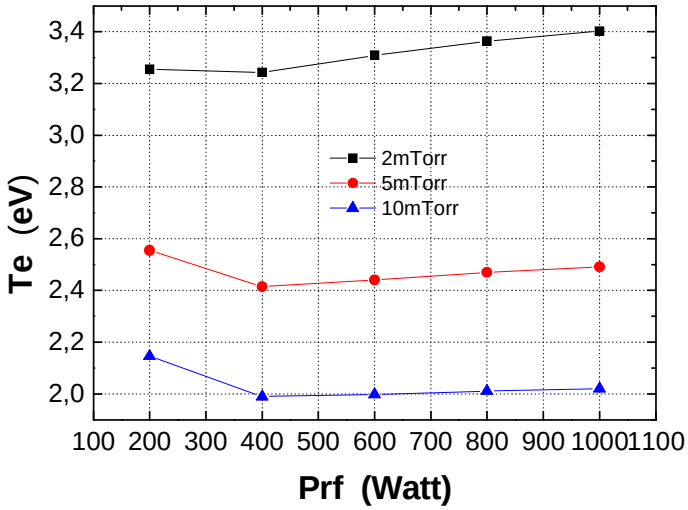

Figure 3. Electron temperature variation with power for pressure ranging from 2 to 10 mtorr, Q(Cl_2/Ar)=10:10 sccm.

Figure 4 shows the variation of the dissociation percentage of Cl_2 as a function of power and pressure. It is calculated as: $dis(\%) = \frac{x_{Cl2}\ N_o - [Cl_2]}{xCl_2\ N_o} \times 100$, where x_{Cl2} is the fraction of Cl_2, N_o is the initial total concentration in the reactor which is determined as a function of the pressure p using parfait gaz law: $N_o(cm^{-3}) = 3.539\ 10^{16}\ p\ (torr)$. At low power, we observe a high variation of the Cl_2 dissociation rate. Over 600 Watt of pressure, such variation becomes low. Noting that the dissociation rate of Cl_2 decreases with the pressure [32-33]. In addition to ions, determination of atomic chlorine density as a function of the operating parameters is useful to determine the Cl flux in the etching process. Such parameter is introduced (see below) as input data in the etching model.

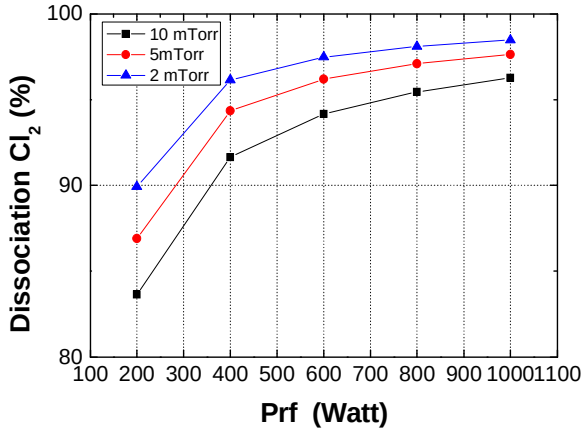

Figure 4. Dissociation percentage of Cl_2 as a function of power and pressure, Q(Cl_2/Ar)=10:10 sccm.

In figure 5, we present, the variation of the chlorine density [Cl] with power for pressure ranging from 2 to 10 mtorr. The increase of such parameter with power is due to the increase of the dissociation rate of molecular chlorine (figure 4).

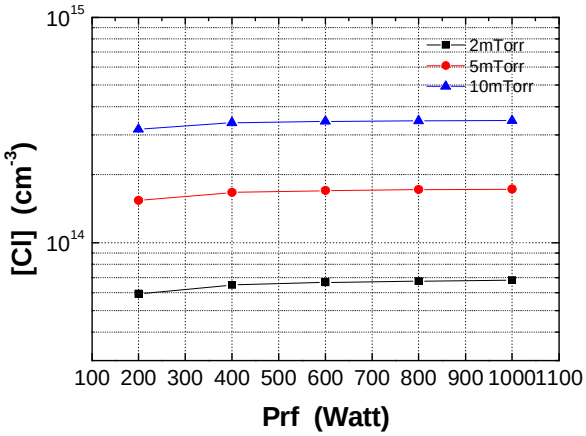

Figure 5. Atomic chlorine density variation with power, Q(Cl_2/Ar)=10:10 sccm.

In low pressure ICP, the role of the plasma surface interaction is very important in the transport study of both charged and neutral species created in the plasma. In our 0D kinetic model, the loss term of atomic chlorine by diffusion mechanism is introduced using Chantry theory [29]. This term is assumed proportional to the recombination coefficient γ_{Cl} on the surface (equation 3). The impact of γ_{Cl} (reaction 17) on the transport phenomena is done in order to understand the mechanisms of the neutral interactions on the surface and their effects on the plasma discharge behaviour. Figure 6 shows the effect of the variation of the recombination coefficient γ_{Cl} on the electron density variation for 2 and 5 mtorr of pressure, 1000 watt of RF power and 10 sccm for both Cl_2 and Ar flow rates. Two regimes can be identified: for γ_{Cl} lower

than 0.01, we observe a slow diminution of [ne] with γ_{Cl}; from 0.01 to 1, the diminution of [ne] with γ_{Cl} becomes very fast. In the case of the [Cl^-] evolution with γ_{Cl} (figure 7-a), we observe a fast increase of [Cl^-] for γ_{Cl} from 0.001 to 0.1. Beyond 0.1 a stability of [Cl^-] is observed by varying γ_{Cl}. On the other hand, for γ_{Cl} less than 10^{-2} electron density [n_e] is less sensitive to the pressure. This tendency changes when γ_{Cl} takes values up to 10^{-2}. We can also observe that γ_{Cl} has an important effect on the electronegativity of Cl_2/Ar plasma discharge. Indeed, figure 7-b shows that in the operating conditions mentioned above (P_{RF}=1000 watt and $Q_{Cl2/Ar}$=10:10 sccm), Cl_2/Ar plasma is all the more electronegative than γ_{Cl} is higher because of the increase of the [Cl_2] (figure8) and consequently the attachment phenomena leading to the augmentation of the [Cl^-].

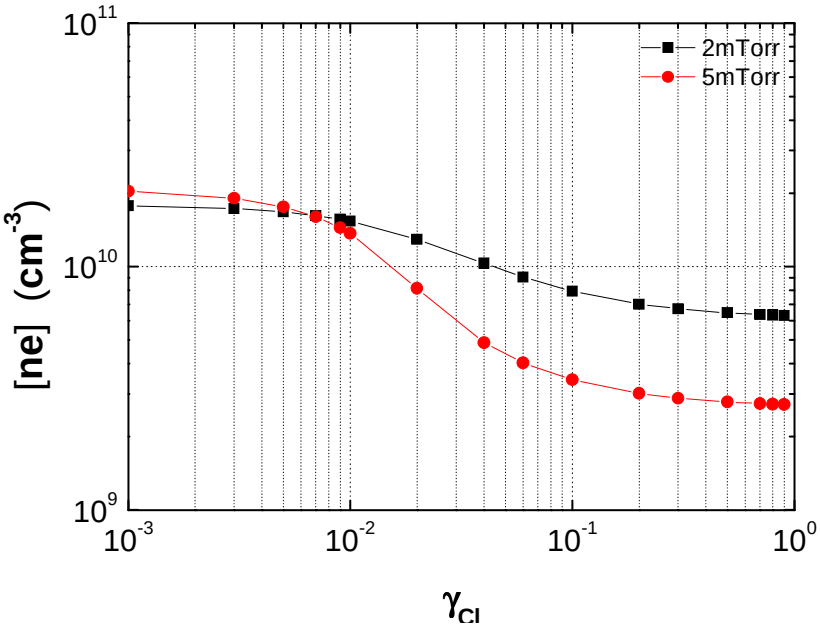

Figure 6. Effect of the recombination coefficient of chlorine on the electron density variation.

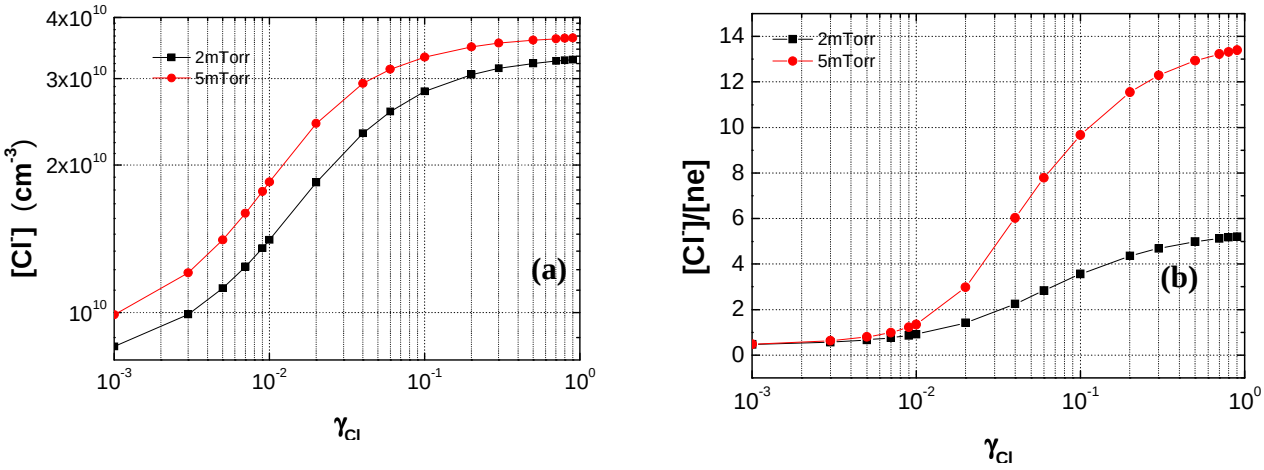

Figure 7. (a), (b): $[Cl^-]$ and $[Cl^-]/[ne]$ evolutions with recombination coefficient of Cl.

Figure 8 presents the Cl_2 density variation as a function γ_{Cl}. For γ_{Cl} lower than 0.2, $[Cl_2]$ increases by increasing γ_{Cl}. Over 0.2, a low increase of $[Cl_2]$ is observed. Noting that for both pressures 2 and 5 mTorr, $[Cl_2]$ is lower than that the initial Cl_2 density $[Cl_2]_o$ for γ_{Cl}=0.04 because of the high Cl_2 dissociation rate (figure 4). Furthermore, high values of atomic chlorine are observed when γ_{Cl} is less than 0.01 due to the high dissociation of Cl_2. Beyond this value; we observe a decrease of [Cl] (figure 9) due to the increase of the loss term on the surface of the Cl (reaction 17).

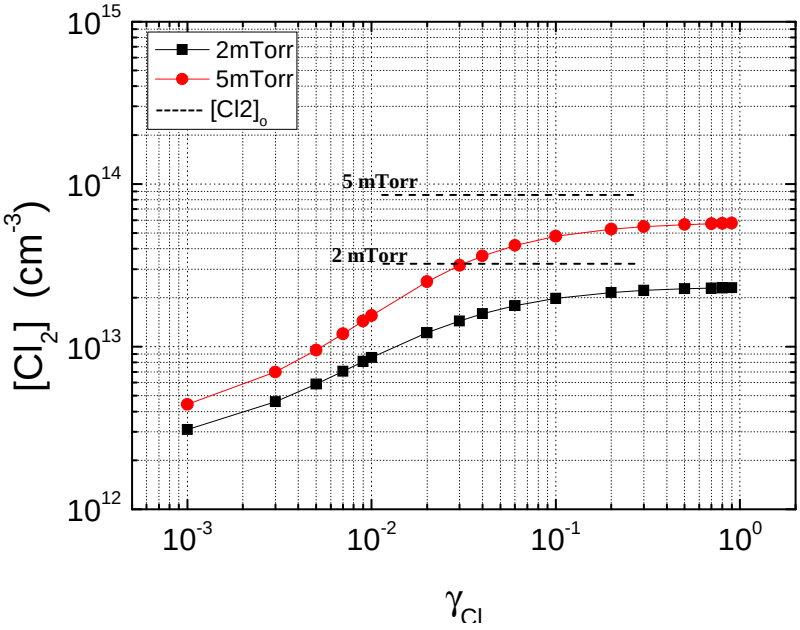

Figure 8. Effect of the recombination coefficient of chlorine on the molecular chlorine density variation. $[Cl_2]_o$ is the chlorine initial density when the plasma is off.

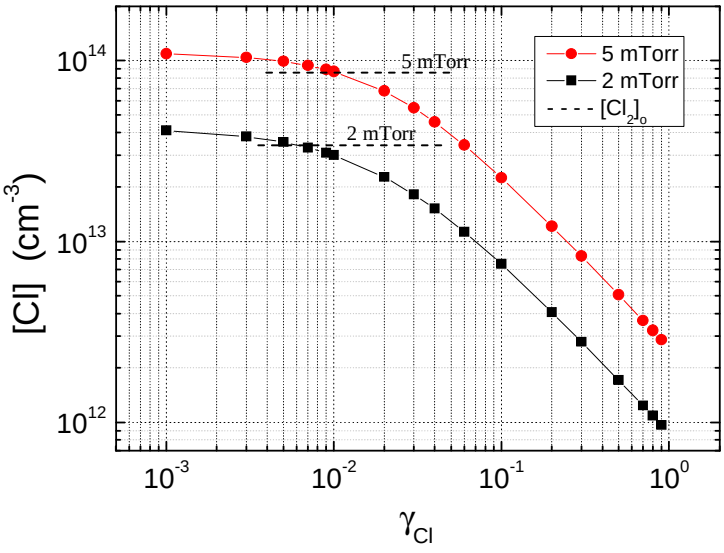

Figure 9 Effect of the recombination coefficient of chlorine on the atomic chlorine density variation. $[Cl_2]_o$ is the chlorine initial density when the plasma is off.

Figure 10 presents the comparison between the simulation and the experiment concerning the electron density and the electron temperature as a function of RF power for 2 mtorr of pressure and $Q_{Cl2/Ar}$=16:4 sccm. For electron density, a less difference is obtained between the simulation and the experiment (figure 10-a). For the electron temperature, a small deviation of the simulated curve from the experiment is observed which is still lesser than 1 eV. However, a good tendency is obtained. The average electron density is expected to be smaller (i) due to its radial decrease within the diffusion chamber, from the centre to the wall, as observed in probe measurements; (ii) due to its axial decrease, from the source to the substrate holder.

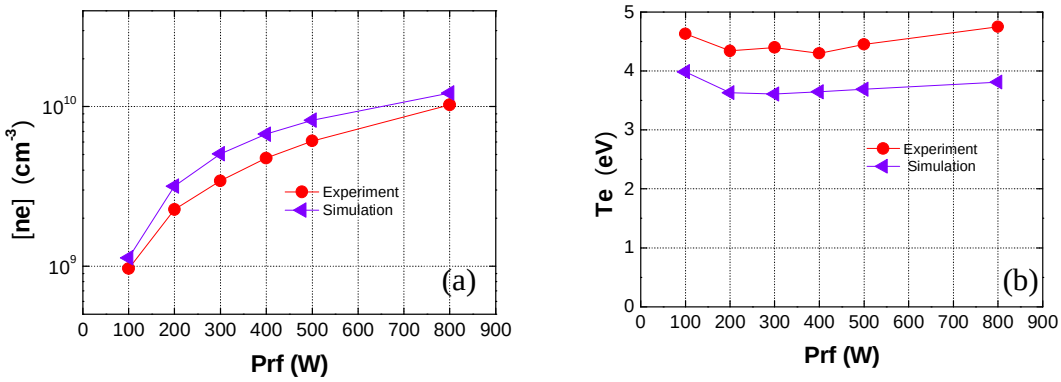

Figure 10. Comparison between the simulation and the experiment. (a) electron density variation with power, (b): electron temperature with power, p= 2 mtorr, $Q_{Cl2/Ar}$=16:4 sccm.

3. Etching model

The model of InP etching by Cl_2/Ar plasma is based on the Monte-Carlo approach. Contrary to the dynamic molecular approach [34-35], the Monte-Carlo kinetic approach permits to use a large etched surface. This method is already used by representing the initial etched InP material under a simple cubic network which the indium and phosphor are randomly placed [36] to respect the amorphous structure in the shallow layers existing near the surface. The transformation from monocrystalline to amorphous structure in the shallow layers is mainly caused by the ion bombardment [36].

In our new version of etching model, we consider the realistic representation of InP etched material based on the zinc-blende structures. Figure 11 presents the initial etched InP where N_x, N_y and N_z represent the lattice number along x, y and z directions respectively.

Two reactive species are taken into account in our InP etching model, atomic chlorine and ion. The main steps of our etching module are summarized as follow: We start by giving the Cl and ion fluxes which are calculated with the global kinetic model as a function of the operating conditions (RF power, pressure, Cl_2/Ar flow rates..). By generating a random number, we select one of the considered precursors. If the neutral species is selected (Cl in our case) then, two random numbers are generated to select its random position (x,y). the z position is chosen on the non occupied plane over the InP surface. The neutral particle is moved into the surface InP sites until encountered occupied nearest neighbour ACl_x sites (A=In or P and x=0-3) in the 1/8 of the InP lattice (sub-cub) of the zinc blende structure. Inside this sub-cube, Cl can adsorb, desorb or jump to one of the nearest neighbour sub-cube. The adsorbed site ACl_{x+1} can chemically desorb

(chemical etching). When the ion is selected, the sputtered indium and phosphorous sites are randomly selected as a function of their sputtering yields.

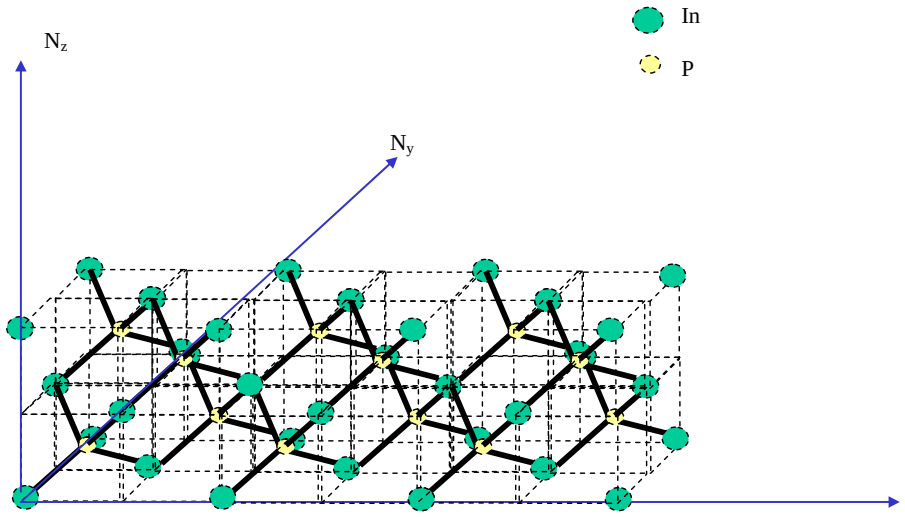

Figure 11. Initial representation of InP (zinc blende structure)

3.1. Precursor transport

Knowing the neutral and ion fluxes ($\Gamma_{ion+} = \Gamma_{Ar+} + \Gamma_{Cl_2^+} + \Gamma_{Cl^+}$) calculated from the global kinetic model, we define time step Δt corresponding to average time between two incident etchant precursors:

$$\Delta t = \frac{1}{S \cdot \Gamma_T} \tag{9}$$

where Γ_T is the total flux of precursors and S is the InP etched surface. To determine which precursor j (Cl or ion) is selected, a random number R is generated and is compared to the flux fraction $X_j = \frac{\Gamma_j}{\Gamma_T}$. Cl is selected for $R \le X_{Cl}$ and ion for $X_{Cl} < R \le 1$.

3.2. Chlorine surface interaction

The probability of each process is defined as a function of surface energies associated to each process by considering Arrhenius law:

$$P_{i,j} = \frac{exp\left(-\frac{E_{i,j}}{KT_s}\right)}{exp\left(-\frac{E_{ads,j}}{KT_s}\right) + exp\left(-\frac{E_{des,j}}{KT_s}\right) + exp\left(-\frac{E_{mig,j}}{KT_s}\right)} \tag{10}$$

where $E_{i,j}$ is the surface energy associated to the process i (i=adsorption, desorption, migration) on the j^{th} site (j=ACl_x, x=0-2). Chemical etching process may occur after the

formation of the ACl_{x+1} by adsorption of Cl on ACl_x. The chemical etching probability is defined as:

$$P_{chem,j} = p_o \cdot exp\left(-\frac{E_{etch,j}}{K \cdot Ts}\right) \quad (11)$$

where $E_{etch,j}$ is the desorption energy of the j^{th} species (j=ACl_x, x=1-3), p_o is a constant and T_s is the surface temperature.

The main difficulty to develop the plasma surface interaction is the lack of the data base concerning the surface parameters such as adsorption and desorption energies of all the formed sites on the etched surface. Table3 presents the surface kinetic of the etched InP under Cl and ion fluxes and their associated surface energies. These are calculated by Jenichen et al [37] using molecular models for local surface structures and the density functional method. The migration energy of Cl is assumed independent of the ACl_x neighbour sites and it is estimated at 1.3 eV.

3.3. Ion InP sputtering model

The energetic ion transport study in InP substrate volume is very complex and requires introducing the linear cascade regime theory [38]. It is not easy to combine our neutral kinetic Monte-Carlo approach with linear cascade regime. Nevertheless, a semi-empirical expression giving the sputtering yield versus the ion energy is used [39]:

$$Y(\alpha, E_{ion}) = \alpha \cdot B \cdot \left(\sqrt{E_{ion}} - \sqrt{E_{th}}\right) \quad (12)$$

where α is the modulation coefficient associated to the site ACl_x (x=0-3). For x=0, α=1 while it is higher than 1 for x>0. B is estimated using TRIM code [38] (table 3).

Neutral (Cl) InP surface interactions				
Surface kinetic reactions	**Adsorption energy (eV)**	**Desorption energy (eV)**	**Etching energy (eV)**	**Migration energy (eV)**
Cl + In → InCl	**1.2**	**1.7**	**1.5**	**1.3**
Cl + InCl → $InCl_2$	**2.8**	**1.7**	**2.79**	**1.3**
Cl + $InCl_2$ → $InCl_3$	**0.473**	**1.7**	**0.35**	**1.3**
Cl + P → PCl	**2.**	**1.7**	**2.48**	**1.3**
Cl + PCl →PCl_2	**1.2**	**1.7**	**1.14**	**1.3**
Cl + PCl_2 → $InCl_3$	**1.2**	**1.7**	**0.057**	**1.3**
Ion sputtering mechanisms				
	B ($eV^{-1/2}$)	**Eth(eV)**	**α**	
ion + In → In	**0.02**	**0**	**1**	
ion+ InCl → InCl	**0.02**	**0**	**3**	
ion + $InCl_2$ → $InCl_2$	**0.02**	**0**	**3**	
ion + $InCl_3$ → $InCl_3$	**0.02**	**0**	**7**	
ion + P → P	**0.011**	**0**	**1**	
ion + PCl →PCl	**0.011**	**0**	**5**	
ion + PCl_2 → $InCl_2$	**0.011**	**0**	**5**	
ion + PCl_2 → $InCl_2$	**0.011**	**0**	**10**	

Table 3. Surface parameters of etched InP under neutral particles (chlorine) and ions .

3.4. Simulation results

One of the advantages of our etching model is to give information about the structural properties of the etched InP in the early stage. Figure 12 presents the etch rate evolution versus time for RF power of 1000 watts, 2 mtorr of pressure, 100 V of V_{DC}, 10:10 sccm of the Cl_2/Ar flow rates and 180 ^oC of substrate temperature. The calculation of the Cl and ion fluxes from the global kinetic model gives $\Gamma_{Cl}=5\ 10^{17}\ cm^{-2}\ s^{-1}$ and $\Gamma_{ion+}= 5.4\ 10^{16}\ cm^{-2}\ s^{-1}$.

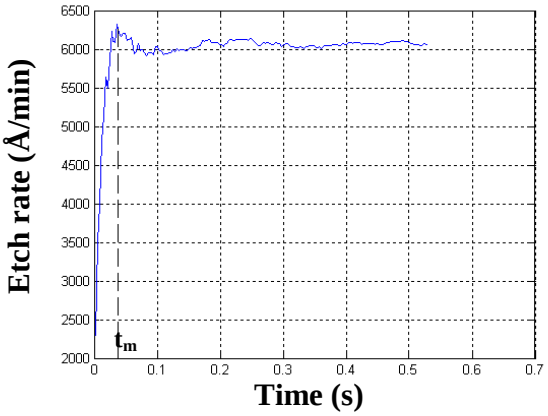

Figure 12. Etching rate evolution with etch time at the early stage

For $t<t_m$ (t_m~0.04 s), the etch rate increases with time until it reaches a maximum value. Beyond this value, a steady state regime is observed. The increase of the etch rate with time for $t<t_m$ is due to the increase of the coverage rate on the adsorbed chloride sites on the surface (figure 13) leading to the increase of the ion neutral synergy of etching. Beyond t_m, we observe a stability of this coverage rate (figure 13) leading to the stability of the etch rate.

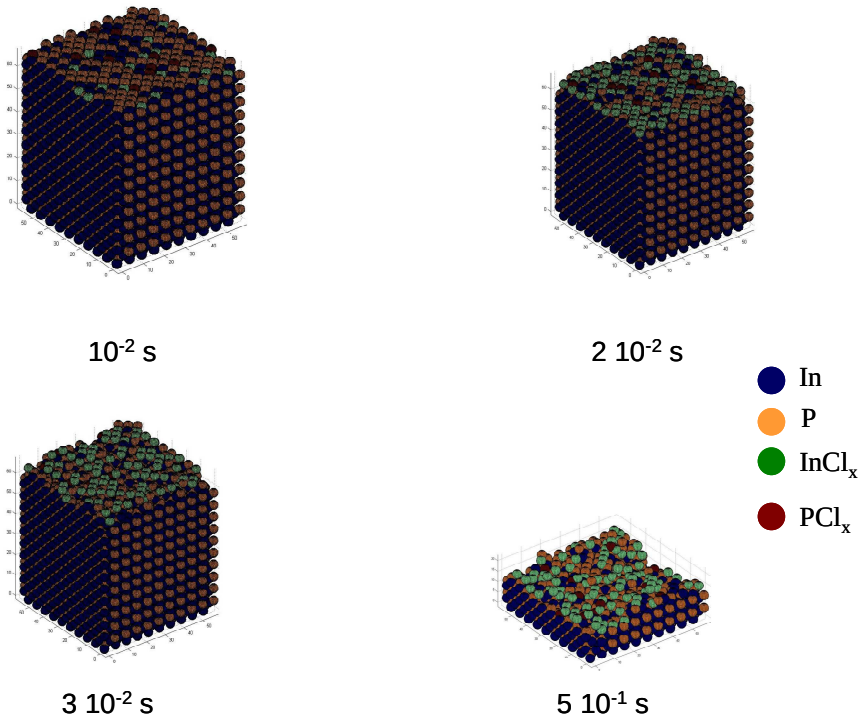

Figure 13. Chemical composition evolution of the etched surface versus etch time

Figure 14 shows the variation of the Roughness rate evolution with time. Contrary to the etch rate that begins to stabilize at t=0.04 s, the RMS is stabilized at 0.4 s. The control of the roughness becomes an important challenge as the miniaturization of the optoelectronic devices progress. So it is important to know more about the mechanisms of the RMS evolution versus the operating conditions.

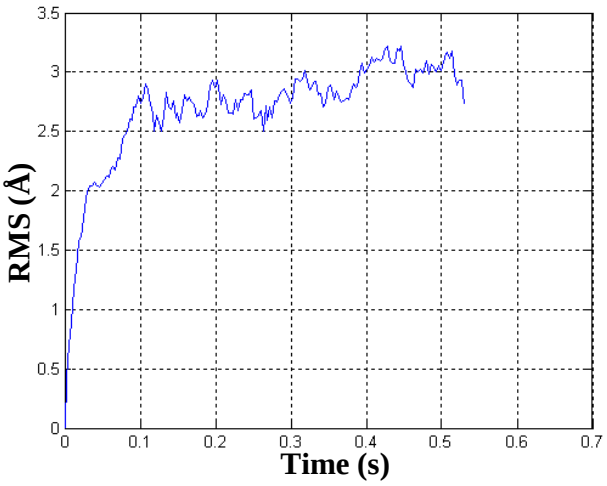

Figure 14. Variation of RMS versus etch time.

Figure 15 presents relative RMS variation versus the pressure for P_{RF}=1000 watts, V_{DC}=100 V, $Q_{Cl2/Ar}$=10/10 sccm and T_s=180 °C. The relative RMS is defined as:

$$RRMS(\%) = \frac{RMS}{t_{ech}} \times 100 \qquad (12)$$

where t_{ech} is the InP etched thickness. RMS and t_{ech} are calcundlated at t=0.5 s. The simulation result shows a diminution of the RRMS with the pressure. It varies from 12.8 % for p=2 mtorr to 4.8 % for p=10 mtorr. This can be explained by the diminution of the ion to chlorine flux ratio (figure 16). Indeed, Γ_{ion}/Γ_{Cl} passes from 0.1 for 2 mtorr to 0.025 for 10 mtorr. The increase of the ion bombardment is a source of the etched surface roughness enhancement.

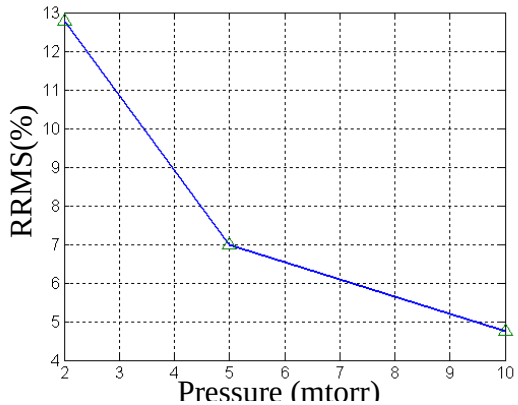

Figure 15. Variation of the RRMS with pressure

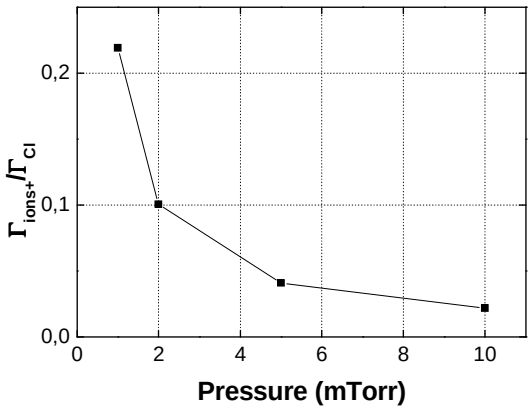

Figure 16. Ion to chlorine flux ratio versus pressure.

4. Conclusion

Gas phase kinetic model for Cl_2-Ar ICP plasma discharge has been developed to investigate the plasma characteristics under operating conditions. The model based on the 0D approach allows to predict average densities of species produced in Cl_2/Ar plasma discharge. Simulation results show that the electronegativity of Cl_2-Ar plasma measured by calculating $[Cl^-]/[ne]$ decreases with increasing RF power and decreasing pressure. A minimum value of the electron temperature is observed at 400 watt. Furthermore, we have analyzed the effect of the surface recombination coefficient of atomic chlorine on the plasma neutral and charged species transport phenomena. The simulation results show that in low pressure, the surface parameters play an important role in the transport phenomena of charged and neutral species created in Cl_2/Ar plasma discharge. A satisfactory agreement between the simulation and the experiment concerning the electron density and the electron temperature evolutions with power are obtained for recombination coefficient of atomic chlorine γ_{Cl} fixed at 0.04. The later is consistent with that estimated experimentally.

On the other hand, a preliminary study concerning the impact of the operation conditions on the etched surface properties is presented. Our attention is particularly paid on the early stage study of the plasma surface interactions where we showed the effect of the correlation between of the RRMS and ion to neutral flux ratio evolutions with pressure.

Acknowledgments:

The authors thank Dr. Sophie Bouchoule and Dr. Lina Gatilova of LPN-CNRS for the electron density and temperature measurements. Part of this work has been supported by Agence Nationale de la Recherche in the frame of ANR-09-BLAN-0019 INCLINE project.

References

[1] P. Strasser, R. Wüest, and F. Robin, A. Forchel, J. Vac. Sci. Technol. B 25, 387-393 (2007).
[2] S. Samukawa, Microelectronic Engineering 53, 69-76 (2000).
[3] S Inoue, K Kajikawa, Mater. Sci. Eng. B103 170-176 (2003).
[4] C. F. Carlström, R. van der Heijden, F. Karouta, R. W. van der Heijden, H. W. M. Salemink, E. Van der Drifft, *J. Vac. Sci. Technol. B 24, (2006).*
[5] A. Xing, M. Davanco, D. J. Blumenthal, E. L. Hu, *J. Vac. Sci. Technol. B 22, 70-73 (2004).*
[6] A. P. Mahorowala, H. H. Sawin, J. Vac. Sci. technol. B 20 1077-1083 (2002).
[7] A. Blauw, E. Van Der Drift, G. Marcos, A. Rhallabi, *J. of Appl. Phys. 94, 6311 (2003).*
[8] G. Marcos, A. Rhallabi, P. Ranson, J. Vac. Sci. Technol. B, 22, No. 4, (2004).
[9] M. A. Vyvoda, M. Li, D. B. Graves, J. Vac. Sci. Technol. B 18, 820-833 (2000).
[10]F. Pommereau, L. Legouezigou, S. Hubert, Sainson, J. P. Chandouineau, S. Fabre, G.H. Duan, B. Lombardet, R. Ferrini, R. Houdre, *J. Appl. Phys. 95, 2242 (2004).*
[11] M. Fujita, A. Sugitatsu, T. Uesugi, S. Noda, *Jap. J. of Appl. Phys., Part 2*, 43, 11A, (2004).
[12] A.P. Milenin, C. Jamois, T. Geppert, U. Gosele, R.B. Wehrspohn, *Microelec. Engin. 81, 15–21 (2005).*
[13] J. W. Lee, E.S. Lambers, C.R. Abernathy, S. J. Pearton, R.J. Shul, F. Ren, W. S. Hobson, C. Constantine, *Mater. Sci. in Semi. Proc. 1, 65-73 (1998).*
[14] J. Lu, X. Meng, A. J. Spring Thorpe, F.R. Shepherd, M. Poirier, *J. Vac. Sci. technol. A 22, 1058-1061 (2004).*
[15] B.Liu, J.P. Landesman, J.L. Leclercq, A.Rhallabi, S. Guilet, C. Cardinaud, F. Pommereau, M.Avella, M.A. González, J. Jiménez, *Mat. Sci. in Semicon. Proc., 9, 1-3, 225-229 (2006).*
[16]K. Nishikawa, T. Oomori, K. Ono, J. Vac. Sci. Technol. B 17 127-137 (1999).
[17] F. Neuilly, J. P. Booth, L. Vallier, J. Vac. Sci. Technol. A 20, 225-229 (2002).
[18] M.V. Malyshev, V. M. Donnelly, S. Samukawa, *J. Appl. Phys. 84 1222-1229 (1998).*
[19] M. V. Malyshev, V. M. Donnelly, *J. Appl. Phys. 87, 1642-1649 (2000).*
[20] M. V. Malyshev, V. M. Donnelly, *J. Appl. Phys. 84, 137-145 (1998).*
[21] M. V. Malyshev, N. C. M. Fuller, K. H. A. Bogart, and V. M. Donnelly, I. P. Herman, *J. Appl. Phys. 88 2246-2251 (2000).*
[22] S. Yonemura, K. Nanbu, K. Sakai, Jpn. J. Appl. Phys. **41**, 6189-6196 (2002).
[23] K. Nanbu, T. Morimoto, M. Suetani, IEEE Trans. on Plasma Sci. 27, 1379 – 1388 (1999).
[24] A.M. Efremov, G. H. Kim, J. G. Kim, A.V. Bogomolov, C.I. Kim, Microelec. Enginee. 84, 136-143 (2007).
[25] T. J. Sommerer, M. J. Kushner, J. Vac Sci. Technol. B 10 2179-2187 (1992).
[26] A. Rhallabi, Y. Catherine, IEEE Trans. on Plasma Sci, 19,(1991).
[27] C. Lee, M. A. Lieberman, J. Vac. Sci. Technol. A 13, 368-380 (1995).
[28] C. Lee, D. B. Graves, M. A. Lieberman, D. W. Hess, *J. electrochem. Soc. 141, 1547 (1994).*
[29] P. J. Chantry, J. Appl. Phys. 62, 1141 (1987).
[30] M. V. Kurepa, D. S. Belie, *J. Phys. B. 11, 3719 (1978).*
[31]M. A. Lennon, K. L. Bell, H. B. Gilbody, J. G. Hughers, A. E. Kingston, M. J. Murray, F. J. Smith, *J. Phys. Chem. Ref. Data 17, 1285 (1988).*
[32] T Czerwiec, F Greer, D B Graves, J. Phys. D: Appl. Phys. 38, 4278–4289 (2005).
[33] N. C. M. Fuller, Irving P. Herman, J. Appl. Phys., 90, 3182-3191 (2001).
[34] M. E. Barone, D. B. Graves, *J. Appl. Phys. 78, 6604 (1995).*
[35] H. Yamada, S. Hamaguchi, J. Appl. Phys., 96, 6147-6152 (2004).
[36] L. Houlet, A. Rhallabi, G. Turban, J. Vac. Sci. Technol. A 17, 2598 (1999).

[37] A. Jenichen, C. Engler, Surf. Sci. 561, 171-182 (2004).
[38] J. F. Ziegler, TRIM (the Transport of Ions in Matter), IBM-Research, 28-0, Yorktown, NY 10598.
[39] G. Marcos, A. Rhallabi, P. Ranson, Appl. Surf. Sci. 254, 3576–3584 (2008).
[40] S. Bouchoule, G. Patriarche, S. Guilet, L. Gatilova, L. Largeau, and P. Chabert, J. Vac. Sci. Technol. B 26, 666 (2008).
[41] G.A. Curley, L. Gatilova, S. Guilet, S. Bouchoule, G. S. Gogna, N. Sirse, S. Karkari, J-P. Booth, J. Vac. Sci. Technol. A 28, 360 (2010).
[42] R. Chanson, N. Vaissière, A. Rhallabi, C. Cardinaud, M.-C. Peignon, S. Bouchoule, paper CTP.00021, 63rd Annual Gaseous Electronics Conference and 7th International Conference on Reactive Plasmas, GEC-IRCP 2010, Paris, France, October 4-8, (2010).
[43] P. C. Cosby, H. Helm, SRI Report, PYU 1147/MP 92-280 (1992).
[44] G. L. Rogoff, J. M. Kramer, R. B. Piejak, IEEE Trans. Plasma Sci. PS-14, 103 (1986).
[45] R. A. Gottscho, G. R. Scheller, T. Intrator, D. B. graves, J. Vac. Sci. Technol. A6, 1393 (1988).
[46] G. R. Scheller, R. A. Gottscho, T. Intrator, D. B. Graves, J. Appl. Phys. 64, 4384 (1988).
[47] G. R. Scheller, R. A. Gottscho, D. B. Graves, T. Intrator, J. Appl. Phys. 64, 598 (1988).
[48] D. Rapp, P. Englander-Golden, J. Chem. Phys. 43, 1464 (1965).
[49] L. R. Peterson, J. E. Allen, Jr., J. Chem. Phys. 56, 6068 (1972).
[50] D. Margreiter, H. Deutsch, T. D. Mark, Contrib, Plasma Phys. 30, 487 (1990).
[51] P. S. Ganas, J. Appl. Phys. 63, 277 (1988).
[52] N. L. Bassett, D. J. Economou, J. Appl. Phys. 75, 1931 (1994)
[53] L. A. Gundel, D. W. Setser, M. A. A. Clyne, J. A. Coxon, W. Nip, J. Chem. Phys. 64, 4390 (1976).